sLZIP functions as a key modulator of bone remodeling by regulating the crosstalk between osteoblasts and osteoclasts

Jesang Ko

jesangko@korea.ac.kr

Korea University https://orcid.org/0000-0002-7609-9719

Sungyeon Park

Korea University

Jeonghan Kim

Catholic University of Korea College of Medicine

Article

Keywords: osteoporosis, bone remodeling, cell therapy, sLZIP

Posted Date: March 7th, 2024

DOI: https://doi.org/10.21203/rs.3.rs-3972073/v1

Additional Declarations: (Not answered)

Abstract

Human small leucine zipper protein (sLZIP) regulates differentiation of both osteoblasts (OBs) and osteoclasts (OCs). However, the regulatory role of sLZIP in bone remodeling and its involvement in bone disorders remain unclear. In this study, we investigated the role of sLZIP in bone remodeling and its significance in the development of cell therapies for the treatment of bone diseases. sLZIP increased bone mass in an osteoporosis mouse model. However, bone mass was lower in mesenchymal stem cell-specific murine LZIP-1/2 knockout (Osx-LZIP-1/2$^{fl/fl}$) mice than in control LZIP-1/2$^{fl/fl}$ mice. Osx-LZIP-1/2$^{fl/fl}$ mice showed delayed bone fracture healing in osteoporosis compared with control mice. Conditioned medium (CM) of OBs differentiated from adipose-derived stem cells (ADSCs) in Osx-LZIP-1/2$^{fl/fl}$ mice attenuated OC formation and migration of bone marrow-derived macrophages. However, CM of OCs from sLZIP transgenic mice induced OB differentiation and migration. sLZIP regulates secretion of OC-derived sphingosine-1-phosphate, which induces OB differentiation. sLZIP also regulates OB-derived WNT16, which inhibits OC differentiation. Therefore, sLZIP functions as a key modulator of the crosstalk between OBs and OCs and promotes bone remodeling and fracture healing in osteoporosis. In addition, sLZIP-overexpressing ADSCs promoted bone formation and repair in osteoporosis. sLZIP is an excellent target for the stem cell-based treatment of osteoporosis.

INTRODUCTION

Bone remodeling is a continuous growth process that maintains bone structure by removing and repairing damaged bones and regulating mineral homeostasis through bone-resorbing osteoclasts (OCs) and bone-forming osteoblasts (OBs)[1]. An imbalance in bone remodeling leads to aging-related bone diseases such as osteoporosis, followed by bone porosity and fragility fractures[2]. Osteoporosis treatments are classified into two categories: anabolic treatments, which generate fresh bone tissue, and antiresorptive treatments, which reduce bone resorption and inhibit bone turnover to stimulate OBs[3]. Parathyroid hormones are used as anabolic treatments for osteoporosis; however, their use is limited to 2 years due to adverse effects[4]. Bisphosphonates were first used as antiresorptive agents for osteoporosis; however, their long-term use causes osteonecrosis in the jaw and increases the risk of esophageal cancer[5, 6]. Denosumab, a specific receptor activator of nuclear factors κB ligand (RANKL) monoclonal antibody, inhibits bone resorption, but patients treated with denosumab often suffer side effects such as dyspnea, back pain, muscle pain, and bone pain[7]. Therefore, dual functional drugs targeting both mechanisms may have superior therapeutic effects; however, no such medication is currently available.

Bone remodeling involves the constant regeneration and resorption of bones to maintain bone homeostasis. Bone remodeling consists of three phases: i) initiation of bone resorption by OCs in the damaged region of the bone, ii) transition from catabolism to anabolism, and iii) bone formation by OBs. The conversion phase of the remodeling cycle refers to the process linking bone resorption and formation, termed coupling[8]. There are two types of coupling factors: those derived from OCs and those derived from OBs. These coupling factors serve as messengers for communication between OBs and OCs

during bone remodeling[9]. Sphingosine-1-phosphate (S1P), WNT10, and collagen triple helix repeat containing 1, which are OC-derived coupling factors, regulate bone formation through crosstalk with OBs[10]. S1P is synthesized via phosphorylation by sphingosine kinase 1/2 (SPHK1/2) and plays an important role in bone development and metabolism[11, 12]. OB-derived coupling factors, including RANKL, osteoprotegerin, semaphorin-3A, sclerostin, and WNT16 communicate with OCs and induce bone resorption[13, 14, 15]. Therefore, a better understanding of the molecular mechanisms regulating bone remodeling and the crosstalk between OBs and OCs is important for developing better approaches for preventing and treating metabolic bone disorders.

The human small leucine zipper protein (sLZIP) is an isoform of LZIP (also known as CREB3). The murine isoforms of sLZIP and LZIP are LZIP-1 and – 2[16]. sLZIP functions as a transcription factor that controls the proliferation, migration, and invasion of various cancer cells[17, 18, 19]. sLZIP also regulates the differentiation of both OBs and OCs[20, 21]. sLZIP induces OB differentiation by serving as a co-activator of run-related transcription factor 2 (RUNX2), a key factor of OB differentiation and a co-repressor of peroxisome proliferator-activated receptor γ2 (PPARγ2), which regulates adipocyte and OB differentiation[20]. sLZIP also increases the nuclear factor of activated T cells, cytoplasmic 1 (NFATc1) transcriptional activity in bone marrow-derived macrophages (BMMs), leading to OC differentiation[21]. Although sLZIP plays an important role in both OB and OC differentiation, the molecular mechanism of bone remodeling remains unknown. In this study, we investigated the regulatory role of sLZIP in bone remodeling and its efficacy in the development of therapeutic agents for metabolic bone disorders.

RESULTS

sLZIP promotes bone regeneration and inhibits bone mass reduction in osteoporosis

sLZIP induces OB differentiation by inhibiting PPARγ2, a negative regulator of OB differentiation, and promotes bone formation[20]. Therefore, we investigated the effects of sLZIP on bone regeneration in a mouse model of osteoporosis. To investigate whether sLZIP is involved in the regulation of bone mass in osteoporosis, we generated osteoporosis mouse models via ovariectomy (OVX) surgery. OVX mice showed a uterine atrophy phenotype and uterine weight reduction compared to sham mice (Fig. S1a). Results of micro-CT (μCT) analysis showed that osteoporosis induced by OVX surgery was characterized as low bone mass in OVX mice compared to sham mice (Fig. 1a). sLZIP TG mice showed high bone mineral density (BMD), trabecular bone volume (BV)/total bone volume (TV), trabecular thickness (Tb.Th), and trabecular bone number (Tb.N) compared to wild type (WT) mice, whereas trabecular separation (Tb.Sp) was low in sLZIP TG mice compared to WT mice (Fig. 1a, b). The bone mass of OVX sLZIP TG mice was restored to of the level observed in sham WT mice (Fig. 1a, b). These results indicate that sLZIP promotes bone regeneration and inhibits bone mass reduction in osteoporosis.

Deletion of sLZIP reduces bone mass and impedes osteoporosis recovery

Bone marrow-derived mesenchymal stem cells (BM-MSCs) are multipotent stromal cells that differentiate into various lineages. *Sp7* (Osx) is used as a specific target of MSCs[22]. To investigate the role of sLZIP in bone regeneration in osteoporosis, we generated MSC-specific sLZIP conditional knockout (KO) mice by crossing Osx-cre and murine LZIP-1/2$^{fl/fl}$ mice and determined the mRNA expression of murine LZIP-1/2 in several tissues. sLZIP KO (Osx-LZIP-1/2$^{fl/fl}$) mice showed decreased mRNA expression of murine LZIP-1/2 in MSCs compared with control LZIP-1/2$^{fl/fl}$ mice (Fig. S1b). sLZIP KO mice showed a reduced trabecular mass in the OVX group (Fig. 2a). Quantitative analyses revealed that BMD, BV/TV, Tb.Th, and Tb.N were lower in sLZIP KO mice than in LZIP-1/2$^{fl/fl}$ mice, whereas Tb.Sp was higher in sLZIP KO mice than in LZIP-1/2$^{fl/fl}$ mice (Fig. 2a). These results indicate that the deletion of sLZIP reduces bone mass and impedes recovery from osteoporosis. As sLZIP promoted bone formation *in vivo*, we investigated the effect of sLZIP on OB differentiation *in vitro.* ADSCs were isolated from fat pads of sLZIP-KO mice and differentiated into OBs. Alkaline phosphatase (ALP) staining, activity analysis, and alizarin red S (ARS) staining revealed that ADSCs from sLZIP KO mice showed decreased OB differentiation compared to ADSCs from LZIP-1/2$^{fl/fl}$ mice (Fig. 2b, c). In addition, the mRNA expression levels of OB differentiation markers, including ALP (*ALPL*), osteocalcin (*BGLAP*), Osx (*Sp7*), and col1a1 (*COL1A1*), were lower in ADSCs from sLZIP KO mice than in those from LZIP-1/2$^{fl/fl}$ mice (Fig. 2d). These results indicate that the deletion of sLZIP reduces bone mass and negatively affects recovery from osteoporosis.

sLZIP induces bone fracture healing and regulates bone remodeling in osteoporosis

Because bone fractures frequently occur in osteoporosis[23], we investigated whether sLZIP is involved in bone fracture healing. To examine the effects of sLZIP on bone fracture healing, we generated a bone fracture model by drilling a portion of the femur in osteoporotic mice. A drill hole defect model was selected to simultaneously mimic bone fractures and avoid nonunion fractures[24]. Seven weeks after the OVX surgery, holes were drilled in the right femur of the mice. After 2 weeks, the femurs were collected (Fig. 3a). Quantitative analysis of bone fracture healing in the OVX group revealed that sLZIP TG mice showed faster callus formation and an increased volume of hard callus-containing bone in the defect region compared with WT mice (Fig. 3b). sLZIP TG mice also exhibited increased cortical thickness and tissue mineral density in the defect region compared with WT mice (Fig. 3c). However, sLZIP KO mice showed decreased callus volume and formation compared to control mice in both sham and OVX groups (Fig. 3d). In addition, the cortical thickness and tissue mineral density were lower in sLZIP-KO mice than in control mice in both groups (Fig. 3f). These results indicate that sLZIP induces bone fracture healing and regulates bone remodeling in osteoporosis. Activation of OBs and OCs is involved in bone remodeling during fracture healing. They play vital roles in the callus and bone formation[25, 26]. Therefore, we examined the levels of OBs and OCs on the surface of transiently formed calli at the site of a mouse

femur defect during bone fracture healing. Results of tartrate-resistant acid phosphatase (TRAP) staining showed that sLZIP TG mice exhibited increased $TRAP^+$ cells on the callus surface in the defective region compared to WT mice in both the OVX and sham groups (Fig. 3f). However, the activated OCs on the callus surface decreased in sLZIP KO mice in both groups (Fig. 3f). These results indicated that sLZIP increases bone resorption by inducing OC activation during bone healing. We investigated the effects of sLZIP on the activation of bone formation during fracture healing. To evaluate the activated OBs, mouse femurs were stained with an ALP staining solution. The results showed that ALP^+ OBs increased in sLZIP TG mice compared to WT mice in the sham group, and sLZIP TG mice showed accelerated bone formation compared to WT mice in the OVX group (Fig. 3g). Compared to sLZIP TG mice, OVX sLZIP KO mice showed decreased ALP^+ cells on the callus surface of the defective region in both groups, indicating that the deletion of sLZIP delayed bone fracture healing by inhibiting callus formation and reducing OC and OB activation in osteoporosis (Fig. 3g). Overall, these results suggest that sLZIP promotes bone resorption and formation during bone fracture healing.

sLZIP functions as a modulator of the crosstalk between OBs and OCs

Bone remodeling, which plays a crucial role in bone repair, is a complex process regulated by crosstalk between bone formation and resorption[27]. Because sLZIP is involved in bone fracture healing and callus formation by activating both OBs and OCs, we postulated that sLZIP modulates bone remodeling by regulating the crosstalk between OBs and OCs. ADSCs and BMMs were isolated from mice and differentiated into OBs and OCs, then the conditioned media of OBs (OB-CM) and OCs (OC-CM) were collected and treated to BMMs and ADSCs, respectively (Fig. 4a). TRAP staining and activity analysis showed that OB-CM from sLZIP TG mice promoted osteoclastogenesis compared with that from WT mice (Fig. S2a and Fig. 4b), whereas OB-CM from sLZIP-KO mice decreased the population of $TRAP^+$ cells compared to that from control mice (Fig. S2b and Fig. 4c). We also examined the effect of sLZIP-mediated OC-CM on OB differentiation. ADSCs isolated from WT mice were treated with the OC-CM obtained from sLZIP-TG mice. The results showed that OC-CM from sLZIP TG mice had increased ALP activity compared to that from WT mice (Fig. S2c and Fig. 4d). In addition, the mRNA expression of OB differentiation markers was increased by OC-CM from sLZIP TG mice compared to WT mice (Fig. S2d). These results indicated that sLZIP modulates OB-OC crosstalk. The migration of MSCs to the bone surface and pre-OCs to the injured region is crucial for bone remodeling and fracture healing[28, 29]. Osteogenesis begins with MSC recruitment at the site of bone remodeling, followed by cell proliferation[30]. Because sLZIP regulates the crosstalk between OBs and OCs, we investigated whether sLZIP affects cell migration and proliferation during bone remodeling. The results of the transwell migration assay showed that OB-CM from sLZIP TG mice increased the migration of pre-OCs compared with that of WT mice (Fig. 4e). In contrast, OB-CM from sLZIP KO mice showed decreased migration of pre-OCs compared to that from $LZIP\text{-}1/2^{fl/fl}$ mice (Fig. 4f). However, the CM of undifferentiated OBs (undiffer-CM) from WT and sLZIP TG mice did not affect pre-OC migration (Fig. 4e, f). OB precursor cells were co-cultured with OC-CM

from WT and sLZIP TG mice to examine the effect of sLZIP on their migration. OC-CM from sLZIP TG mice showed increased migration of OB precursor cells compared to that from WT mice (Fig. 4g). Next, we investigated whether the OC-CM from sLZIP TG mice affected the proliferation of OB precursor cells. However, we found no significant differences between OC-CM from WT and sLZIP TG mice (Fig. S2e). These results indicated that sLZIP-induced CM increased cell migration during bone remodeling without affecting cell proliferation.

sLZIP modulates bone remodeling by regulating the crosstalk between OBs and OCs

sLZIP regulates the crosstalk between OBs and OCs by inducing the coupling factors

As sLZIP is involved in OB–OC crosstalk during bone remodeling, we investigated whether sLZIP affects coupling factor secretion. We examined the effect of sLZIP on the secretion of OC-mediated coupling factors during OC differentiation. S1P is synthesized through phosphorylation by SPHK1/2 and is involved in bone formation and survival[12, 31]. Therefore, we examined the mRNA expression of SPHK1 during OC differentiation from progenitor cells. The mRNA level of SPHK1 was increased by sLZIP during OC differentiation, whereas the mRNA level of SPHK2 remained unaffected (Fig. 6a). sLZIP TG mice showed increased SPHK1 protein expression during OC differentiation compared with WT mice (Fig. 6b). To examine the effect of sLZIP on S1P synthesis by SPHK1, we performed SPHK1 activity assays. SPHK1 activity was increased in mature OCs derived from sLZIP TG mice compared to that in WT mice (Fig. 6c). The S1P level also increased by 13% in mature OCs derived from sLZIP TG mice compared to that in WT mice (Fig. 6d). These results indicated that sLZIP induces S1P secretion by stimulating SPHK1 activity in OCs. S1P is involved in bone formation by upregulating cyclooxygenase-2 (COX-2) via the p38/ERK pathway[31]. We investigated whether sLZIP-induced S1P affects activation of the p38/ERK pathway in ADSCs. OC-CM derived from sLZIP TG mice induced the phosphorylation of p38 and increased COX-2 expression compared to WT mice (Fig. 6e). To confirm whether sLZIP-induced S1P was involved in COX-2-mediated bone formation, we used the S1P receptor inhibitor JTE-013. OC-CM derived from sLZIP TG mice showed increased COX-2 expression compared to that in undifferentiated mice; however, COX-2 expression was decreased by JTE-013 in a dose-dependent manner (Fig. 6f). We also examined the effects of sLZIP on the OB-mediated secretion of coupling factors during OB differentiation. *WNT16* mRNA expression was reduced in OBs from sLZIP TG mice compared to those of WT mice (Fig. 6g). These results indicate that sLZIP regulates crosstalk between OBs and OCs by inducing coupling factors.

sLZIP overexpressing ADSCs promote bone formation and bone repair in osteoporosis

We investigated whether sLZIP could be used in cell therapy to treat osteoporosis. To examine the effect of ADSCs isolated from sLZIP TG mice (sLZIP TG-ADSCs) on osteoporosis, we performed a drilling assay on the right femur of WT mice and then administered each type of ADSCs via intravenous injection to each group (Fig. S3a). The results showed that cortical thickness (Ct.th) and tissue mineral density (TMD) were increased by sLZIP TG-ADSCs compared to WT-ADSCs (Fig. S3b). sLZIP TG-ADSCs showed increased BMD, BV/TV, and Tb.th compared to WT-ADSCs (Fig. S3c). These results indicate that sLZIP TG-ADSCs have potential as a cell therapy for bone fractures and reduced bone mass. C-X-C motif receptor 4 (CXCR4) plays a role in MSC migration to the bone marrow, demonstrating its potential as a therapeutic agent for osteoporosis[32]. To optimize the efficiency of cell therapy, we generated lentiviruses overexpressing CXCR4 and sLZIP (LV-CXCR4/sLZIP) and infected them with ADSCs isolated from WT mice. Seven weeks after OVX surgery, each group was injected with PBS, WT-ADSCs, or LV-CXCR4/sLZIP-ADSCs. After 10 days, bone formation was analyzed using μCT (Fig. 7a). LV-CXCR4/sLZIP-ADSCs showed elevated Ct.th, TMD, BMD, BV/TV, and Tb.th compared to those of LV-CXCR4/mock-ADSCs, whereas Tb.Sp was reduced (Fig. 7b, c). To examine the effect of LV-CXCR4/sLZIP-ADSCs on bone fracture healing, we performed a drilling assay on the right femur of mice after OVX surgery; four groups were injected with PBS, WT-ADSCs, and virus-infected ADSCs (Fig. 8a). The 3D images showed that mice injected with WT-ADSCs and LV-CXCR4/mock-ADSCs showed enhanced bone recovery in the defect areas compared to those in the PBS group (Fig. 8b). The LV-CXCR4/sLZIP-ADSC group exhibited more effective bone repair than the WT-ADSC and LV-CXCR4/Mock-ADSC groups (Fig. 8b). The results of μCT revealed that WT-ADSCs and LV-CXCR4/Mock-ADSCs increased Ct.th and TMD, along with elevated BMD and Tb.N compared to PBS (Fig. 8b, c). These results showed that mice injected with LV-CXCR4/sLZIP-ADSCs exhibited increased bone formation and fracture recovery compared to the control groups. These findings indicate that sLZIP-overexpressing ADSCs promote bone formation and repair in osteoporosis and have the highest ability to treat osteoporosis and fracture recovery.

DISCUSSION

Medicines for osteoporosis have made substantial progress as novel treatment strategies but have many adverse effects and no cure has been achieved[33]. Therefore, understanding the molecular mechanisms underlying osteoporosis treatment is important. Osteoporosis is a common bone remodeling disorder[34]. Bone remodeling is performed by a functional and anatomic structure known as the basic multicellular unit (BMU). The BMU refers to the anatomical structure that involves new bone filling by OBs in the space absorbed by the OCs[35]. Previous studies suggest that sLZIP not only regulates the balance between adipogenesis and osteogenesis but also induces the differentiation of BMMs into OCs by promoting NFATc1 transactivation[20, 21]. Because sLZIP functions as a modulator of both bone resorption and formation, we speculated that sLZIP is an essential factor for regulating BMU and bone remodeling.

sLZIP KO mice showed reduced bone mass compared to control mice in the OVX group, whereas the bone mass in OVX sLZIP TG mice was restored to that of sham WT mice. These results indicated that sLZIP prevents bone loss in patients with osteoporosis. Osteoporosis with attenuated bone mass is

followed by bone porosity and fragility fractures[2, 36, 37, 38]. Therefore, we investigated the effect of sLZIP on the healing of osteoporosis-induced bone fractures. sLZIP KO mice showed reduced bone repair compared with control mice in the OVX group. We confirmed that bone mass was reduced by OVX. However, OC formation was lower in the OVX group than in the sham group. These results can be explained by clinical surveys showing that osteoporotic patients have delayed fracture healing compared to non-osteoporotic patients when fractures occur[39]. Several studies have reported on this topic. PDK1 deletion in OCs delays fracture union and repair by reducing callus resorption[40]. The bone fracture model in OVX mice showed decreased callus formation and BMD compared with sham mice[24]. OCs are responsible for removing soft calluses and forming hard calluses during the bone fracture healing process[41]. Therefore, reduced OC content on the callus surface in OVX mice delayed callus formation caused by osteoporosis and decreased OC activity. Typically, both anabolic and anti-bone-resorptive osteoporosis treatments act through a single pathway[33]. Denosumab, a monoclonal antibody against RANKL, also inhibits OC activity[42]. Because one-pathway functional drugs have many side effects, dual functional drugs targeting both mechanisms may have superior therapeutic effects. However, currently available drugs are less known. Therefore, alternative treatments for osteoporosis are urgently needed.

MSCs are undifferentiated cells with self-renewal and multilineage differentiation abilities, and are closely related to the progression of osteoporosis[43]. Accordingly, MSCs have been studied over the past few decades for their potential to establish therapeutic strategies for various pathophysiological dysfunctions in degenerative medicine[44]. MSCs have promising applications in the treatment of osteoporosis. Direct transplantation of MSCs into OVX mice promotes osteogenic differentiation[45]. When bone marrow-derived MSCs were injected into OVX mice via the tail vein, MSC-transplanted OVX mice showed significantly increased BMD, Tb.N, Tb.th, and BV[45]. Homing is the first phase of bone repair, in which MSCs migrate to the bone marrow to fulfill local functions and aid in recovery[32]. CXCR4 plays a role in homing MSCs to the bone marrow[32]. OVX mice injected with MSCs co-transfected with RANK-Fc and CXCR4 showed increased BMD compared with sham mice[46]. However, MSC transplantation also has side effects owing to excessive bone formation. Therefore, studies on dual-function drugs using CXCR4-MSC are needed.

Our results indicated that sLZIP accelerates bone fracture healing by promoting osteoclastogenesis and osteoblastogenesis. OB-CM derived from sLZIP-KO mice show reduced BMM migration and OC differentiation. OC-CM derived from sLZIP KO mice showed decreased OB precursor cell migration and differentiation. The results of the co-culture study showed that sLZIP regulates bone remodeling by controlling the crosstalk between OBs and OCs. These results suggest that sLZIP is a suitable target for controlling both pathways and can provide a molecular mechanism for developing novel cell therapies. Furthermore, we found that LV-CXCR4/sLZIP-ADSCs demonstrated a therapeutic effect by increasing bone formation compared to WT-ADSCs in osteoporotic mice.

The coupling process is vital in bone diseases because pathological bone diseases are caused by the dysregulation of the interplay between OBs and OCs[34]. Therefore, studies on novel coupling factors are

important for osteoporosis treatment, and many studies have been conducted on the coupling factors involved in bone remodeling. S1P synthesized by SPHK1/2 in OCs is secreted and induces bone formation and survival by binding to S1PR, an S1P receptor in the membrane of OBs[12]. OC-derived semaphorin 4D binds to plexin-B1on the surface of OBs and inhibits OB differentiation[47]. Recent studies have reported factors that regulate coupling factors. TGIF1 promotes osteoclastogenesis in OBs by inhibiting semaphorin 3E, an OB-derived coupling factor that suppresses OC differentiation[48]. Although S1P secreted from OCs acts as a coupling factor for OB formation, the molecular mechanisms underlying S1P regulation in OCs remain unclear. In this study, we demonstrated that sLZIP enhances S1P secretion by inducing SPHK1 expression during OC differentiation and that sLZIP-secreted S1P in OCs affects OB differentiation. These results suggest that sLZIP in OCs is essential for regulating S1P, and that sLZIP acts as an important regulator of coupling factors. OB-derived WNT16 reduces osteoclastogenesis by interfering with RANK signaling[38]. We found that sLZIP TG reduced *WNT16* mRNA expression during OB differentiation. These results indicated that sLZIP regulates osteoclastogenesis by inhibiting WNT16 secretion in OBs. Therefore, our findings demonstrated that sLZIP plays an important role as a modulator of coupling factor secretion in both OCs and OBs.

Coupling factors not only act as secreted proteins but also mediate direct cell–cell communication between OBs and OCs. The Ephrin B2 ligand within the OC membrane interacts with EphB4, which is located on the OB membrane. The Ephrin B2/EphB4 axis affects both OBs and OCs. Claudin 11 maintains bone homeostasis via bidirectional EphrinB2/EphB4 signaling[49]. We found that the mRNA levels of Ephrin B2 were increased by sLZIP during differentiation into mature OCs. However, Ephrin B2 deletion in BMMs does not result in any bone abnormalities[50]. Because bone mass is regulated by sLZIP, Ephrin B2 does not contribute to the sLZIP-induced coupling process.

Bone remodeling is a complex process in which various cells interact simultaneously in localized spaces. Drugs currently used to treat osteoporosis disrupt bone homeostasis owing to their excessive absorption and bone formation. Therefore, the key to the treatment of osteoporosis is to reduce the side effects of drugs by targeting two pathways rather than focusing on one. In this study, we demonstrated that sLZIP exerts an osteoprotective effect by promoting bone resorption and formation and functions effectively in restoring bone fractures caused by osteoporosis. This study provides a molecular basis for developing treatments to control bone absorption and formation. Thus, sLZIP is a dual-function medicinal candidate for the treatment of metabolic bone diseases.

MATERIALS AND METHODS

Materials

Dulbecco's modified Eagle's medium (DMEM) was purchased from Thermo Fisher Scientific (Waltham, MA). Eagle's minimum essential medium, alpha modification (α-MEM), and fetal bovine serum (FBS) were obtained from GE Healthcare Life Sciences (Pittsburg, PA, USA). Recombinant human/mouse/rat bone

morphogenetic protein 2 (BMP-2) was obtained from R&D systems, Inc (McKinley Place, NE, USA). L-ascorbic acid, dexamethasone, and β-glycerophosphate were purchased from Millipore (Burlington, MA, USA). Mouse M-CSF was purchased from PeproTech (Rocky Hill, NJ, USA). Mouse RANKL was obtained from R&D Systems, Inc. Type I collagenase was purchased from Millipore (Billerica, MA). The fluorescent mounting medium was obtained from Dako (Santa Clara, CA, USA). Tissue-Tek® O.C.T compound was purchased from Sakura Finetek (Torrance, CA, USA). Antibodies against SPHK1 (G-11) and COX-2 were purchased from Santa Cruz Biotechnology (Dallas, TX, USA).

Ethics statement for animal study

We adhered to the essential procedures specified in the Animal Research: Reporting of In Vivo Experiments (ARRIVE) guidelines to minimize suffering for the experimental animals and ensure appropriate care and welfare. The animal studies were approved by the Ethics Committee of Animal Experiments at Korea University (KUIACUC-2021-0095), and all procedures were performed in strict accordance with the Korea University Guide for the Care and Use of Animals in Laboratory Experiments. The mouse strain C57BL6 were used for the animal study. Mice were purchased from Gyerim experimental animal resource center (Seoul, South Korea) and maintained at 22 ± 2°C and 50 ± 10% humidity under a 12 h light-dark regimen. In all animal studies, mice were anesthetized with isoflurane following the AVMA (American Veterinary Medical Association) guidelines for abdominal laparotomy. Animals were euthanized in strict accordance with ethical guidelines. CO2 was injected into the chamber at a rate of 30–70% charging per minute. After visual confirmation of death, complete euthanasia was induced by exposing the mice to CO2 for an additional minute and death was confirmed by monitoring their heartbeats.

Isolation of primary mouse ADSCs

Primary mouse ADSCs were isolated as previously described[51]. Briefly, 8-week-old mice were euthanized by cervical dislocation. After sterilization with 70% ethanol, the abdominal cavity was opened and the desired fat pad was removed. Fat was incubated with collagenase type I buffer for 60 min. After collagenase digestion, the samples were centrifuged at 300 · g for 5 min at 25°C. Pellets were washed with 1% BSA and centrifuged at 300 · g for 5 min. Collected ADSCs were resuspended in DMEM containing 10% FBS, 100 U/mL penicillin, and 100 μg/mL streptomycin. Cells were plated on a culture dish and cultured in a 37°C humidified incubator containing 5% CO_2. The medium was changed every 2 days until the cells reached 80% confluence.

Isolation of primary mouse BMMs

Mice aged 8–12 weeks were euthanized by cervical dislocation. After sterilization with 70% ethanol, the skin near the femur was clipped outward to expose the hind legs. All muscle tissues were removed from the isolated femurs and tibias. Superior and inferior ends of the isolated bones were cut, and bone marrow cells were flushed out with α-MEM containing 10% FBS, 100 U/mL penicillin, and 100 μg/mL streptomycin using a 10 mL syringe and 24-gauge needle. A single-cell suspension was created by pipetting, and cells were passed through a cell strainer with a 100 μm pore size (SPL Life Science Co.,

Pocheon, South Korea) to remove other bone components. After centrifugation at 200 × g for 3 min at 25°C, cells were resuspended in fresh medium and cultured at 37°C in a humidified incubator containing 5% CO_2.

Cell culture and differentiation

Mouse ADSCs were isolated via sequential collagenase digestion of the fat pad obtained from 8-week-old mice and grown in DMEM containing 10% FBS, 100 U/mL penicillin, and 100 μg/mL streptomycin. For OB differentiation, when the cells reached confluence, differentiation was initiated with DMEM containing 50 μg/mL ascorbic acid and 10 mM β-glycerophosphate for 7–14 days. The differentiation medium was replaced every 2–3 days. Primary BMMs were isolated from long bone-derived bone marrow of mice and maintained in α-MEM containing 10% FBS, 100 U/mL penicillin, and 100 μg/mL streptomycin. After 24 h, floating mouse primary bone marrow cells were separated into two 100 mm culture dishes and treated with 50 ng/mL M-CSF for 3 days. To generate OCs from BMMs, cells were seeded in 12- or 96-well plates containing 50 ng/mL M-CSF for 24 h. Cells were then treated with 30 ng/mL M-CSF and 50 ng/mL RANKL. The media and cytokines were replaced every 2 days.

RNA isolation and quantitative RT-PCR

Mouse primary BMMs at a density of 1.5×10^5 cells/well were seeded on 12-well plates. After RANKL treatment, the cells were rinsed with PBS and detached. Mouse ADSCs were seeded at the density of 8×10^5 cells/well in 12-well plates and were differentiated into OBs for 7 days when the cells reached 80% confluence. Total RNA was isolated using the TaKaRa miniBEST universal RNA extraction kit (Takara Bio Inc., Shiga, Japan), and cDNA was synthesized from the total RNA using PrimeScript™ RT master mix (Takara Bio Inc.) according to the manufacturer's instructions. Quantitative RT-PCR (qRT-PCR) was performed on a LightCycler 480 II (Roche, Basel, Switzerland) using Evagreen-express master mix (Applied Biological Materials, Vancouver, BC, Canada). Semi-qRT-PCR was performed on a T100™ thermal cycler (Bio-Rad, Hercules, CA, USA) using Pfu Plus 5× PCR Master Mix (Elpis Biotech, Inc., Daejeon, South Korea). The primer sequences used for PCR are listed in Table 1.

Table 1
Primer sequences used for qRT-PCR.

mRNA	Primer sequence (Forward)	Primer sequence (Reverse)
mRUNX2	AGGGACTATGGCGTCAAACA	GGCTCACGTCGCTCATCTT
mALP	GGACAGGACACACACACACA	CAAACAGGAGAGCCACTTCA
mCol1a1	GCTCCTCTTAGGGGCCACT	ATTGGGGACCCTTAGGCCAT
mOsterix	GAAAGGGAAGCAGAACCATACTATTTG	TCAGTGGTGTGCCTTCATATTCA
mSHPK1	TGGGCTGTCCTTCAACCTCATACA	AACAGCAGTGTGCAGTTGATGAGC
mSPHK2	AAGCAAGAGAAAGCTGGTCATC	AGTGACAATGCCTTCCCACTCACT
mSEMA4D	CCTGGTGGTAGTGTTGAGAAC	GCAAGGCCGAGTAGTTAAAGAT
mEphrinB2	TCTGTGTCATCGGTTGGCTACGTT	ACAGACGCACAGGACACTTCTCAA
mTRAP	CTGTGCGACATCAACGAAAGG	CCTTGGGAGGCTGGTCTTAAA
msLZIP	GAAGCTCTTGGAGAAGGA	TTCAAGACCCTGCTCTCC
sLZIP	AGCAGCAGCATGTACTCCTCT	AGGCAGCTCCAGCTGGTAAG
mβ-Actin	AACCCTAAGGCCAACCGTGAAAA	AGGATGGCGTGAGGGAGAGCATA

Alizarin red S and alkaline phosphatase staining and activity assay

Mouse ADSCs were differentiated in osteogenic medium for 14 days. Differentiated OBs were fixed with 4% formaldehyde solution for 10 min at 25°C and stained with alizarin red S (ARS) and alkaline phosphatase (ALP) staining solutions. For ARS staining, cells were washed with PBS, and evaluated cell matrix mineralization by staining with 2% ARS solution (Millipore Sigma). For ALP staining, the cells were washed with PBS and stained using a TRACP/ALP double staining kit (Takara Bio Inc.) according to the manufacturer's instructions. For ALP activity analysis, cells were seeded at a density of 4×10^4 cells/well in a 96-well culture plate and cultured in osteogenic medium in a time-dependent manner. The cells were evaluated using a TRACP/ALP assay kit (Takara Bio, Inc.).

Tartrate-resistant acid phosphatase activity and bone resorption assays

For the TRAP activity assay, BMMs were seeded in 96-well culture plates at a density of 1×10^4 cells/well. Three days after OB differentiation, the cells were washed with PBS and evaluated using a TRACP/ALP assay kit (Takara Bio Inc.) according to the manufacturer's instructions. For the bone resorption assay, the same number of cells was seeded on Corning® osteo assay surface 96-well plates (Corning, NY, USA). Five days after OC differentiation, cells were detached using 10% bleach solution for 5 min at 25°C. After washing several times with DDW, the plates were placed in an incubator for 24 h. To quantify

resorption activity, the resorption area (pixels)/total well area (pixels) for five random fields was determined.

Conditioned medium collection

For conditioned medium (CM) collection, mouse BMMs were seeded in 12-well plates at a density of 1.25 × 10^5 cells/well. The cells were differentiated into OCs for 5–7 days using RANKL (50 ng/mL) and M-CSF (30 ng/mL). After OC differentiation, supernatants were collected and centrifuged at 200 × g for 3 min. To collect the OB-CM, mouse ADSCs were seeded in 12-well culture plates at a density of 8 × 10^4 cells/well. The cells were then differentiated into OBs for 7 days. The supernatant was centrifuged at 300 × g for 3 min.

Transwell cell migration

Mouse ADSCs (2 × 10^4 cells/100 μL) were seeded on the top chamber of 24-transwell plates (8 μm pore size; BD Biosciences, San Diego, CA, USA). After 5 h, OC-CM was added to the bottom chamber for 18 h. Mouse BMMs (8 × 10^4 cells/100 μL) were seeded on the top chamber of transwell plates with M-CSF (30 ng/mL). OB-CM was added to the bottom chamber for 24 h. Cells on the lower surface of the membrane were stained with 0.05% crystal violet according to the manufacturer's protocol. The cell counts of the adherent cells were obtained from five randomly selected fields per well, and the values were expressed as the average of the counts.

Cell proliferation

The cell proliferation assay was performed using EZ-cytox DoGenBio (Gyeonggi, South Korea), according to the manufacturer's protocol. Mouse ADSCs were in 96-well plates seeded at a density of 3 × 10^3 cells/100 μL. After 24 h, the cells were incubated with OC-CM for the indicated times. After the medium was removed, the cells were treated with 10 μL of EZ-cytox solution and incubated at 37°C for 30 min. Cell viability was determined by measuring the absorbance at 450 nm.

Sphingosine kinase 1 activity assay

Sphingosine kinase 1 activity was determined using a sphingosine kinase activity assay kit (Echelon, Salt Lake City, UT, USA), according to the manufacturer's instructions. Mouse BMMs were seeded in 12-well culture plates at a density of 1.5 × 10^4 cells/well. After 24 h, BMMs were differentiated into OCs in α-MEM media containing 30 ng/mL M-CSF and 50 ng/mL RANKL for 7 days. The media and cytokines were replaced every 2 days. Protein extracts (30 μg) were incubated with reaction buffer, 100 μM sphingosine, and 10 μM ATP for 30 min at 37°C. Sphingosine kinase 1 activity was measured using SpectraMax®i3x (Molecular Devices, CA, USA).

Co-culture of OBs and OCs

Mouse BMMs and ADSCs were co-cultured either indirectly or directly. To examine the crosstalk between OBs and OCs, an indirect co-culture was performed using either OB-CM or OC-CM. The CM of each cell

line was transferred to WT ADSCs or BMMs for 10–13 days. Indirect co-culture models were evaluated using ALP and TRAP staining. For direct co-culture, ADSCs were co-cultured with BMMs in 96-well plates in DMEM containing M-CSF (30 ng/mL) at an OBs: OCs = 1:1.5. The co-culture models were added to OB or OC medium at 80% confluence. After 7–10 days of co-culture, the cells were evaluated using ALP or TRAP staining.

Enzyme-linked immunosorbent assay (ELISA)

Bone marrow macrophages (BMMs) were isolated from WT and sLZIP TG mice and differentiated for 7 days. OC-CM was collected and S1P levels were measured using a mouse S1P ELISA Kit (MyBioSource, Inc., San Diego, CA, USA) according to the manufacturer's instructions.

sLZIP-overexpressing levtivirus generation and transduction

The sLZIP-overexpressing lentivirus was obtained from Sirion Biotech (Martinsried, Germany). The codon-optimized sequences of mouse CXCR4 and human sLZIP were cloned into the pcLV-CMV-eGFP-T2A-Puro-WPRE plasmid. LV-containing supernatants were produced by the transient transfection of HEK-293T cells. The titer was 10^9 TU/mL. For transduction, ADSCs were seeded in 100 mm culture plates at a density of 1×10^6 cells/plate. After 24 h, cells were incubated in 5% FBS DMEM with 8 μg/mL polybrene and LV-CXCR4/sLZIP. Medium was changed after 16–24 h and infected ADSCs were selected following continuous incubation in DMEM with 10 μg/mL puromycin for 24 h. Prior to experiments, MSCs were cultured 48 h without puromycin.

OVX surgery mouse model

Eight-week-old female mice were randomly divided into two groups: sham control ($n = 4–5$) and OVX surgery ($n = 6–7$). Female mice were ovariectomized under inhalation anesthesia. Anesthesia was induced using 1.8% isoflurane at a rate of 50 mL/min with 1–2% vaporization in the nose. After shaving the hair in the dorsal mid-lumbar area, the dorsal skin was incised and the bilateral ovaries were removed. The wounds were closed with sutures. Sham control mice underwent the same procedure, but the ovaries were not removed. After 6 weeks, the OVX mice were euthanized for further analysis.

Bone-defect mouse model

A bone defect model was generated using 6–8-week-old mice. Prior to surgery, anesthesia was induced using a Somnosuite low-flow anesthesia system (Kent Scientific Co., Torrington, CT, USA) and isoflurane (Hana Pharm Co., Ltd., Seoul, South Korea). Isoflurane was used at 150–200 mL/min with 2.5% vaporization in the induction chamber. Anesthetized mice were maintained using isoflurane at 50 mL/min and 1–2% vaporization in the nose. The right thigh was epilated and sterilized with 70% ethanol and the skin was incised over the lateral femoral aspect to expose muscle. Blunt dissection of the quadriceps was performed to expose the femoral bone. The posterior and anterior cortices of the middle of the femur were perforated (0.6 mm in diameter) by using a drill bit and hand drill (Jeungdo Bio&Plant Co., LTD, Seoul, South Korea), while chilled PBS was irrigated to the site to avoid heat damage. After perforation,

the muscle and skin tissues were repositioned using sutures. The surgical field was disinfected with povidone. The mice were then returned to their cages and administered an analgesic (30 mg/mL ibuprofen diluted in drinking water).

ADSC intravenous injection

For ADSC-based therapeutic experiments, ADSC form WT and TG were collected at 1×10^6 cells/100 μL PBS immediately before intravenous injection. For LV-CXCR4/SLZIP ADSC-based therapeutic experiments, ADSC form WT and ADSC infected with LV-CXCR4 and LV-CXCR4/sLZIP were collected at 1×10^6 cells/100 μL PBS immediately before intravenous injection.

Micro-CT scanning

Mouse femurs were collected after anesthesia. Whole muscles and connective tissues were removed, and the samples were fixed in a 4% paraformaldehyde solution over 1 week at 4°C. Mouse femur was subjected to μCT scanning using SkyScan1172 (Bruker, MA, USA) under the conditions of a source 70 kV voltage, 135 μA current, 0.5 mm Al filter, and 680 ms exposure time. Images were processed using reconstruction software (NRecon v1.6, Data Viewer v1.5) and three-dimensional visualization software (CTvox v2.6), and data analysis was performed using analysis software (CTAn v1.14). After three-dimensional reconstruction, the bone volume/tissue volume (BV/TV) of a 1.604 mm length of cortical bone containing the defect region was automatically calculated using built-in software.

Histological analysis

Mouse femurs were fixed in 4% paraformaldehyde (Sigma-Aldrich) solution at 4°C. After fixation, the samples were decalcified at 4°C for 2 weeks using 5 mL Osteosoft solution (Sigma-Aldrich). However, the samples used for OB staining were not decalcified. The solution was changed every 2–3 days. Samples were soaked in a 30% sucrose (Sigma-Aldrich) solution at 4°C for 24 h and transferred to optimal cutting temperature compound (Tissue-Tek, Sakura Finetek, South-Holland, Netherlands). Samples were then cryo-sectioned into 10 μm-thick slices in the proximal to distal vertical direction and transferred to glass slides. The optimal cutting temperature compound was removed using ethanol, and the samples were subjected to TRAP and ALP staining. After mounting the medium and applying cover slips, the samples were observed and analyzed under a light microscope.

Statistical analysis

All data are presented as the mean ± SEM. Statistical analyses were performed using GraphPad Prism 5 (GraphPad Software, La Jolla, CA, USA). Two-tailed Student's *t*-test results of $P < 0.05$ were considered statistically significant.

Declarations

Data Availability Statement

The data underlying this article will be shared on reasonable request to the corresponding author.

Conflict of Interest Statement

The authors declare no conflicts of interest.

Author Contributions

S. Park and J. Ko participated to conception and design of the experiments and contributed to data analysis and interpretation, and wrote the manuscript. J. Kim contributed to design of the experiments and data analysis. S. Park performed experiments.

Acknowledgments

This work was supported by Basic Science Research Program through the National Research Foundation of Korea (NRF) funded by the Ministry of Science, ICT and Future Planning (NRF-2017R1E1A1A01073955) and the Korea University Grant.

References

1. Yu W, Zhong L, Yao L, Wei Y, Gui T, Li Z, *et al.* Bone marrow adipogenic lineage precursors promote osteoclastogenesis in bone remodeling and pathologic bone loss. J Clin Invest, 131(2): (2021).
2. Raisz LG. Pathogenesis of osteoporosis: concepts, conflicts, and prospects. J Clin Invest, 115(12): 3318–3325 (2005).
3. Zhen G, Dan Y, Wang R, Dou C, Guo Q, Zarr M, *et al.* An antibody against Siglec-15 promotes bone formation and fracture healing by increasing TRAP(+) mononuclear cells and PDGF-BB secretion. Bone Res, 9(1): 47 (2021).
4. Cranney A, Papaioannou A, Zytaruk N, Hanley D, Adachi J, Goltzman D, *et al.* Parathyroid hormone for the treatment of osteoporosis: a systematic review. CMAJ, 175(1): 52–59 (2006).
5. Abrahamsen B. Adverse effects of bisphosphonates. Calcif Tissue Int, 86(6): 421–435 (2010).
6. Watts NB, Diab DL. Long-Term Use of Bisphosphonates in Osteoporosis. J Clin Endocr Metab, 95(4): 1555–1565 (2010).
7. Khosla S, Hofbauer LC. Osteoporosis treatment: recent developments and ongoing challenges. Lancet Diabetes Endocrinol, 5(11): 898–907 (2017).
8. Raggatt LJ, Partridge NC. Cellular and molecular mechanisms of bone remodeling. J Biol Chem, 285(33): 25103–25108 (2010).
9. Han Y, You X, Xing W, Zhang Z, Zou W. Paracrine and endocrine actions of bone-the functions of secretory proteins from osteoblasts, osteocytes, and osteoclasts. Bone Res, 6: 16 (2018).

10. Henriksen K, Karsdal MA, Martin TJ. Osteoclast-derived coupling factors in bone remodeling. Calcif Tissue Int, 94(1): 88–97 (2014).
11. Futerman AH, Hannun YA. The complex life of simple sphingolipids. EMBO Rep, 5(8): 777–782 (2004).
12. Spiegel S, Milstien S. Sphingosine-1-phosphate: an enigmatic signalling lipid. Nat Rev Mol Cell Biol, 4(5): 397–407 (2003).
13. Behar O, Golden JA, Mashimo H, Schoen FJ, Fishman MC. Semaphorin III Is needed for normal patterning and growth of nerves, bones and heart. Nature, 383(6600): 525–528 (1996).
14. Theoleyre S, Wittrant Y, Tat SK, Fortun Y, Redini F, Heymann D. The molecular triad OPG/RANK/RANKL: involvement in the orchestration of pathophysiological bone remodeling. Cytokine Growth Factor Rev, 15(6): 457–475 (2004).
15. Compton JT, Lee FY. A review of osteocyte function and the emerging importance of sclerostin. J Bone Joint Surg Am, 96(19): 1659–1668 (2014).
16. Burbelo PD, Gabriel GC, Kibbey MC, Yamada Y, Kleinman HK, Weeks BS. LZIP-1 and LZIP-2: two novel members of the bZIP family. Gene, 139(2): 241–245 (1994).
17. Kang H, Jang SW, Ko J. Human leucine zipper protein sLZIP induces migration and invasion of cervical cancer cells via expression of matrix metalloproteinase-9. J Biol Chem, 286(49): 42072–42081 (2011).
18. Kim J, Ko J. Human sLZIP promotes atherosclerosis via MMP-9 transcription and vascular smooth muscle cell migration. FASEB J, 28(11): 5010–5021 (2014).
19. Kim Y, Kim J, Jang SW, Ko J. The role of sLZIP in cyclin D3-mediated negative regulation of androgen receptor transactivation and its involvement in prostate cancer. Oncogene, 34(2): 226–236 (2015).
20. Kim J, Ko J. A novel PPARgamma2 modulator sLZIP controls the balance between adipogenesis and osteogenesis during mesenchymal stem cell differentiation. Cell Death Differ, 21(10): 1642–1655 (2014).
21. Kim S, Park S, Kang M, Ko J. The role of small leucine zipper protein in osteoclastogenesis and its involvement in bone remodeling. Biochim Biophys Acta Mol Cell Res, 1867(11): 118827 (2020).
22. Fan Y, Cui C, Rosen CJ, Sato T, Xu R, Li P, *et al.* Klotho in Osx(+)-mesenchymal progenitors exerts pro-osteogenic and anti-inflammatory effects during mandibular alveolar bone formation and repair. Signal Transduct Target Ther, 7(1): 155 (2022).
23. Tu KN, Lie JD, Wan CKV, Cameron M, Austel AG, Nguyen JK, *et al.* Osteoporosis: A Review of Treatment Options. P T, 43(2): 92–104 (2018).
24. He YX, Zhang G, Pan XH, Liu Z, Zheng LZ, Chan CW, *et al.* Impaired bone healing pattern in mice with ovariectomy-induced osteoporosis: A drill-hole defect model. Bone, 48(6): 1388–1400 (2011).
25. Einhorn TA, Gerstenfeld LC. Fracture healing: mechanisms and interventions. Nat Rev Rheumatol, 11(1): 45–54 (2015).

26. Pajarinen J, Lin T, Gibon E, Kohno Y, Maruyama M, Nathan K, *et al.* Mesenchymal stem cell-macrophage crosstalk and bone healing. Biomaterials, 196: 80–89 (2019).
27. Sims NA, Gooi JH. Bone remodeling: Multiple cellular interactions required for coupling of bone formation and resorption. Semin Cell Dev Biol, 19(5): 444–451 (2008).
28. Su P, Tian Y, Yang C, Ma X, Wang X, Pei J, *et al.* Mesenchymal Stem Cell Migration during Bone Formation and Bone Diseases Therapy. Int J Mol Sci, 19(8): (2018).
29. Tang Y, Wu X, Lei W, Pang L, Wan C, Shi Z, *et al.* TGF-beta1-induced migration of bone mesenchymal stem cells couples bone resorption with formation. Nat Med, 15(7): 757–765 (2009).
30. Granero-Molto F, Weis JA, Miga MI, Landis B, Myers TJ, O'Rear L, *et al.* Regenerative effects of transplanted mesenchymal stem cells in fracture healing. Stem Cells, 27(8): 1887–1898 (2009).
31. Ryu J, Kim HJ, Chang EJ, Huang H, Banno Y, Kim HH. Sphingosine 1-phosphate as a regulator of osteoclast differentiation and osteoclast-osteoblast coupling. Embo J, 25(24): 5840–5851 (2006).
32. Jiang Y, Zhang P, Zhang X, Lv L, Zhou Y. Advances in mesenchymal stem cell transplantation for the treatment of osteoporosis. Cell Prolif, 54(1): e12956 (2021).
33. Kennel KA, Drake MT. Adverse effects of bisphosphonates: implications for osteoporosis management. *Mayo Clin Proc*, 84(7): 632–637; quiz 638 (2009).
34. Feng X, McDonald JM. Disorders of bone remodeling. Annu Rev Pathol, 6: 121–145 (2011).
35. Jilka RL. Biology of the basic multicellular unit and the pathophysiology of osteoporosis. Med Pediatr Oncol, 41(3): 182–185 (2003).
36. Zebaze RM, Ghasem-Zadeh A, Bohte A, Iuliano-Burns S, Mirams M, Price RI, *et al.* Intracortical remodelling and porosity in the distal radius and post-mortem femurs of women: a cross-sectional study. Lancet, 375(9727): 1729–1736 (2010).
37. Zheng HF, Tobias JH, Duncan E, Evans DM, Eriksson J, Paternoster L, *et al.* WNT16 influences bone mineral density, cortical bone thickness, bone strength, and osteoporotic fracture risk. PLoS Genet, 8(7): e1002745 (2012).
38. Moverare-Skrtic S, Henning P, Liu X, Nagano K, Saito H, Borjesson AE, *et al.* Osteoblast-derived WNT16 represses osteoclastogenesis and prevents cortical bone fragility fractures. Nat Med, 20(11): 1279–1288 (2014).
39. Gorter EA, Reinders CR, Krijnen P, Appelman-Dijkstra NM, Schipper IB. The effect of osteoporosis and its treatment on fracture healing a systematic review of animal and clinical studies. Bone Rep, 15: 101117 (2021).
40. Xiao D, Zhou Q, Bai Y, Cao B, Zhang Q, Zeng G, *et al.* Deficiency of PDK1 in osteoclasts delays fracture healing and repair. Mol Med Rep, 22(2): 1536–1546 (2020).
41. Schindeler A, McDonald MM, Bokko P, Little DG. Bone remodeling during fracture repair: The cellular picture. Semin Cell Dev Biol, 19(5): 459–466 (2008).
42. Anastasilakis AD, Polyzos SA, Makras P. THERAPY OF ENDOCRINE DISEASE: Denosumab vs bisphosphonates for the treatment of postmenopausal osteoporosis. Eur J Endocrinol, 179(1): R31-

R45 (2018).
43. Berebichez-Fridman R, Montero-Olvera PR. Sources and Clinical Applications of Mesenchymal Stem Cells: State-of-the-art review. Sultan Qaboos Univ Med J, 18(3): e264-e277 (2018).
44. Kolios G, Moodley Y. Introduction to stem cells and regenerative medicine. Respiration, 85(1): 3–10 (2013).
45. Yu Y, Shao B, Zhou Z, Shang F, Shuai Y, Wang X, *et al.* [Role of bone marrow-derived mesenchymal stem cells in treating estrogen deficiency induced osteoporosis]. Xi Bao Yu Fen Zi Mian Yi Xue Za Zhi, 29(12): 1267–1271 (2013).
46. Cho SW, Sun HJ, Yang JY, Jung JY, An JH, Cho HY, *et al.* Transplantation of mesenchymal stem cells overexpressing RANK-Fc or CXCR4 prevents bone loss in ovariectomized mice. Mol Ther, 17(11): 1979–1987 (2009).
47. Negishi-Koga T, Shinohara M, Komatsu N, Bito H, Kodama T, Friedel RH, *et al.* Suppression of bone formation by osteoclastic expression of semaphorin 4D. Nat Med, 17(11): 1473–1480 (2011).
48. Saito H, Gasser A, Bolamperti S, Maeda M, Matthies L, Jahn K, *et al.* TG-interacting factor 1 (Tgif1)-deficiency attenuates bone remodeling and blunts the anabolic response to parathyroid hormone. Nat Commun, 10(1): 1354 (2019).
49. Baek JM, Cheon YH, Kwak SC, Jun HY, Yoon KH, Lee MS, *et al.* Claudin 11 regulates bone homeostasis via bidirectional EphB4-EphrinB2 signaling. Exp Mol Med, 50(4): 1–18 (2018).
50. Zhao C, Irie N, Takada Y, Shimoda K, Miyamoto T, Nishiwaki T, *et al.* Bidirectional ephrinB2-EphB4 signaling controls bone homeostasis. Cell Metab, 4(2): 111–121 (2006).
51. Yu G, Wu X, Kilroy G, Halvorsen YD, Gimble JM, Floyd ZE. Isolation of murine adipose-derived stem cells. Methods Mol Biol, 702: 29–36 (2011).

Figures

Figure 1.

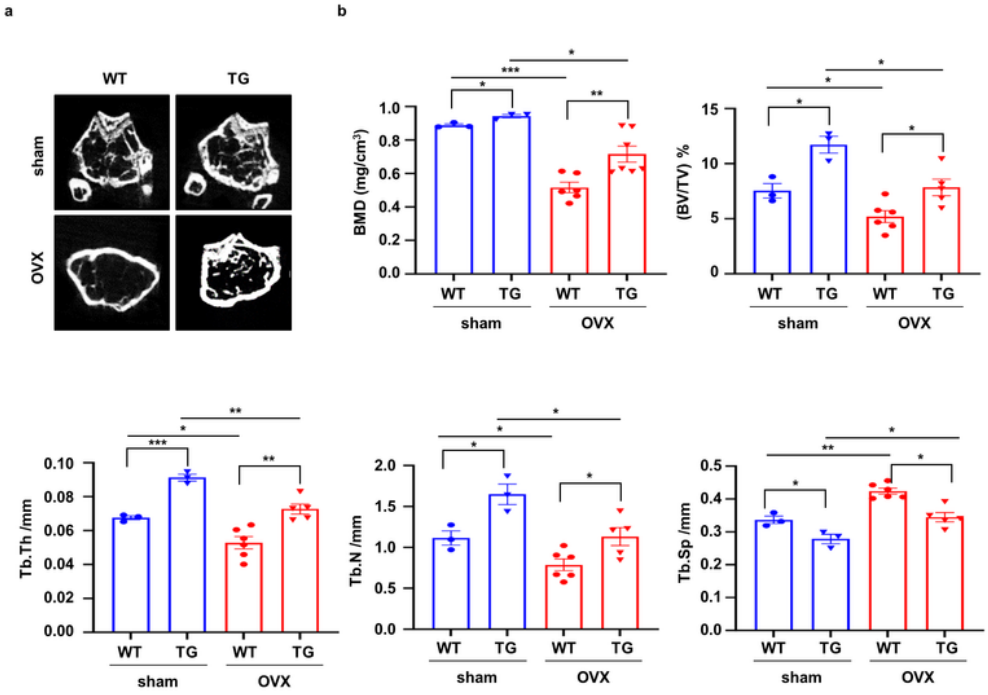

Figure 1

sLZIP promotes bone regeneration and inhibits bone mass reduction in osteoporosis. **a** mCT of trabecular bones in femurs of WT (n = 3) and sLZIP TG (n = 6) mice was performed. Representative μCT two-dimensional images are shown. **b** BMD, BV/TV, Tb.Th, Tb.N, and Tb.Sp were quantified based on μCT image analysis. Error bars: mean ± SEM. *p < 0.05, **p < 0.01, ***p < 0.001 (unpaired, Two-tailed Student's t-test).

Figure 2.

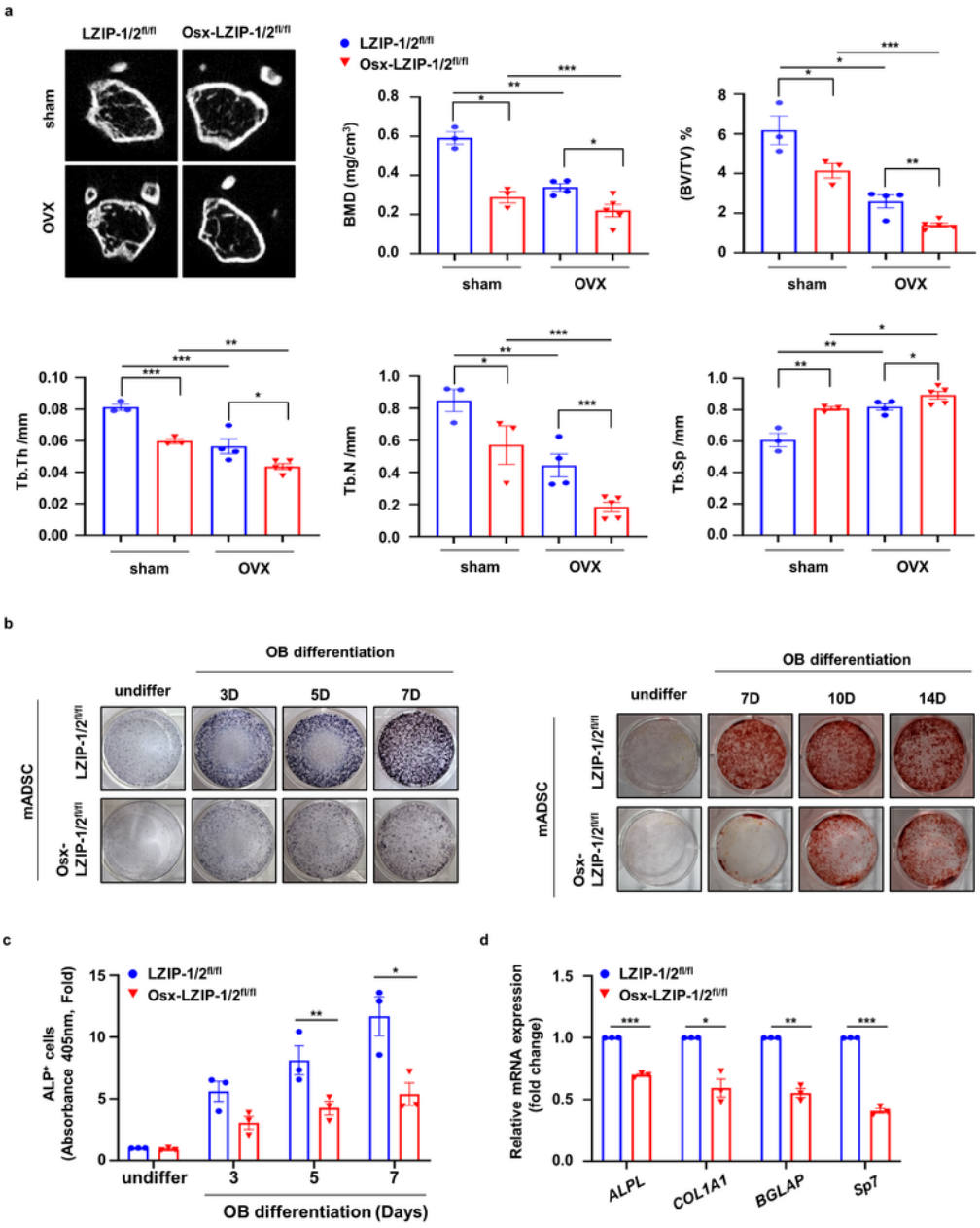

Figure 2

Deletion of sLZIP reduces bone mass and impedes osteoporosis recovery. **a** mCT of trabecular bones in femurs of LZIP-1/2$^{fl/fl}$ (n =3–4) and Osx-LZIP-1/2$^{fl/fl}$ (n = 3–5) mice was performed. Representative μCT two-dimensional images are shown. BMD, BV/TV, Tb.Th, Tb. N, and Tb.Sp were quantified based on μCT image analysis. **b** For ALP staining, ADSCs derived from LZIP-1/2$^{fl/fl}$ and Osx-LZIP-1/2$^{fl/fl}$ mice were seeded at a density of 2 × 10^5 cells/well and differentiated into OBs for 3, 5, and 7 days in osteogenic

medium. For ARS staining, ADSCs isolated from LZIP-1/2$^{fl/fl}$ and Osx-LZIP-1/2$^{fl/fl}$ mice were differentiated into OBs for the indicated time. Cells were stained with 2% ARS solution. **c** ADSCs derived from LZIP-1/2^{flfl} and Osx-LZIP-1/2$^{fl/fl}$ mice were seeded at a density of 4×10^4 cells/well in 96 well plates. ALP activity was quantified using the ALP assay kit. **d** ADSCs derived from LZIP-1/2$^{fl/fl}$ and Osx-LZIP-1/2$^{fl/fl}$ mice were differentiated into OBs for 7 days in osteogenic medium. The mRNA expression level was determined using qRT-PCR, which was performed in triplicate per group. The mRNA level of OB differentiation markers was determined using qRT-PCR, which was performed in triplicate per group. Error bars: mean ± SEM. *$p < 0.05$, **$p < 0.01$, ***$p < 0.001$ (unpaired, Two-tailed Student's *t*-test).

Figure 3.

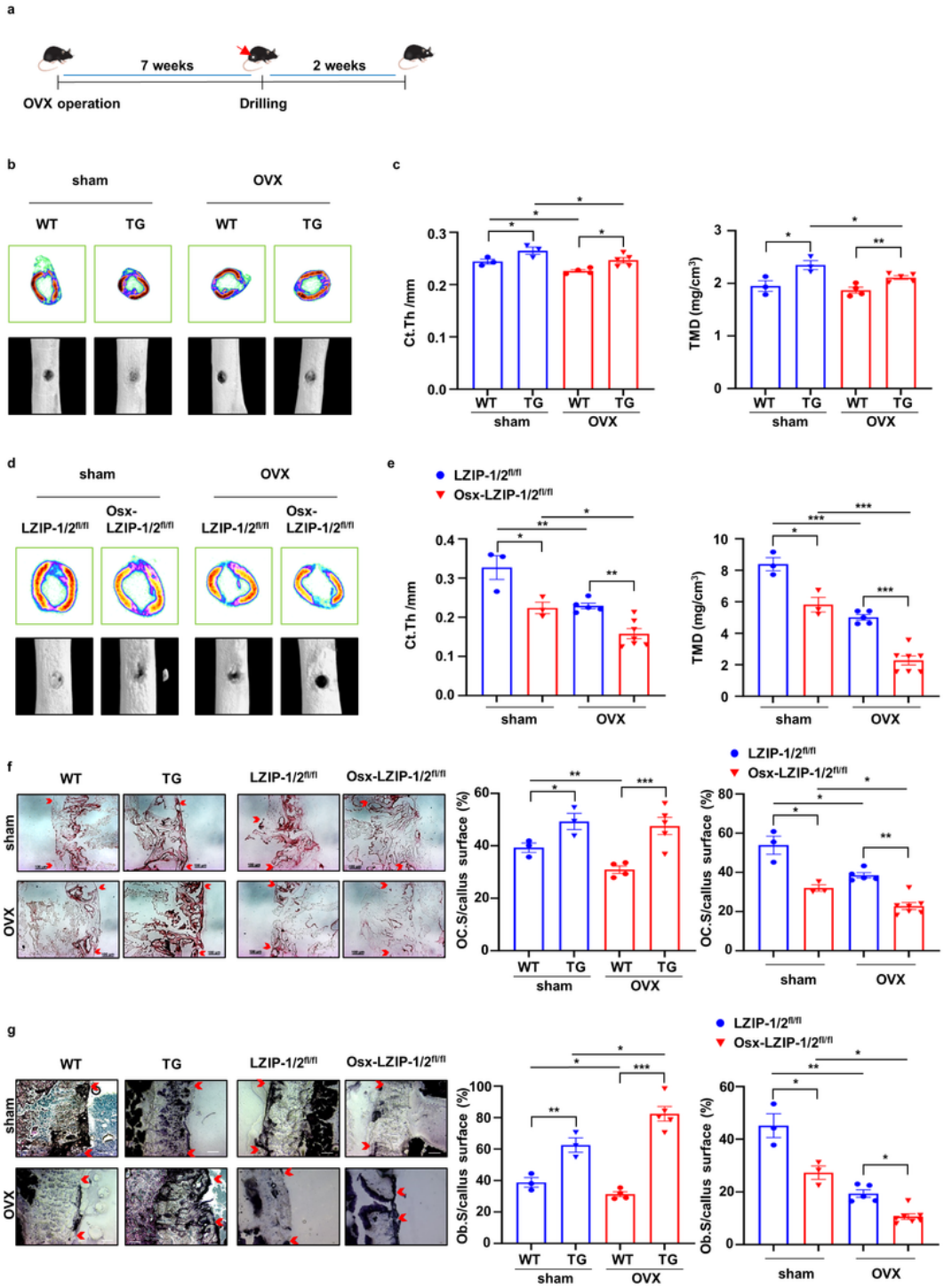

Figure 3

sLZIP induces bone fracture healing and regulates bone remodeling in osteoporosis. **a** Eight-week-old mice were used for OVX surgery. Seven weeks after surgery, mice were anesthetized and underwent surgery to drill holes in the right femur. The mice underwent drill-hole surgery were euthanized via cervical dislocation after 14 days. The right femur was harvested and fixed. **b-e** Representative two- and three-dimensional images were obtained from μCT scanning. **b** Representative 2D images were generated from

μCT analysis after the drill-hole surgery in WT and TG mice. **c** Quantification of Ct.Th and TMD were analyzed using the μCT program (CTAn) **d** Representative 2D images amd 3D images were generated from μCT analysis after the drill-hole surgery in Osx-LZIP-1/2$^{fl/fl}$ and LZIP-1/2$^{fl/fl}$ mice. **e** Quantification of Ct.Th and TMD were analyzed using the μCT program. **f** The mouse femurs were obtained after two weeks of decalcification and the defected region of mouse femurs was cryo-sectioned (8 μm thickness). Decalcified femurs from female WT, sLZIP TG, LZIP-1/2$^{fl/fl}$, and Osx-LZIP-1/2$^{fl/fl}$ mice (n = 3–6) were subjected to TRAP staining. Representative images of callus sections demonstrated bone healing after drill-hole surgery. Scale bar = 100 μm. **g** The mouse femurs were obtained in undecalcified state and the defected region of mouse femurs was cryo-sectioned (8 μm thickness). Undecalcified femurs from female WT, sLZIP TG, LZIP-1/2$^{fl/fl}$, and Osx-LZIP-1/2$^{fl/fl}$ mice (n = 3–6) were subjected to ALP staining. Representative images of callus sections demonstrated bone healing after drill-hole surgery. Scale bar = 100 μm. The ratio of TRAP^{+} and ALP^{+} cell surface area, and the trabecular bone surface area was measured using Image J. Error bars: mean ± SEM. *p < 0.05, **p < 0.01, ***p < 0.001 (unpaired, Two-tailed Student's t-test).

Figure 4.

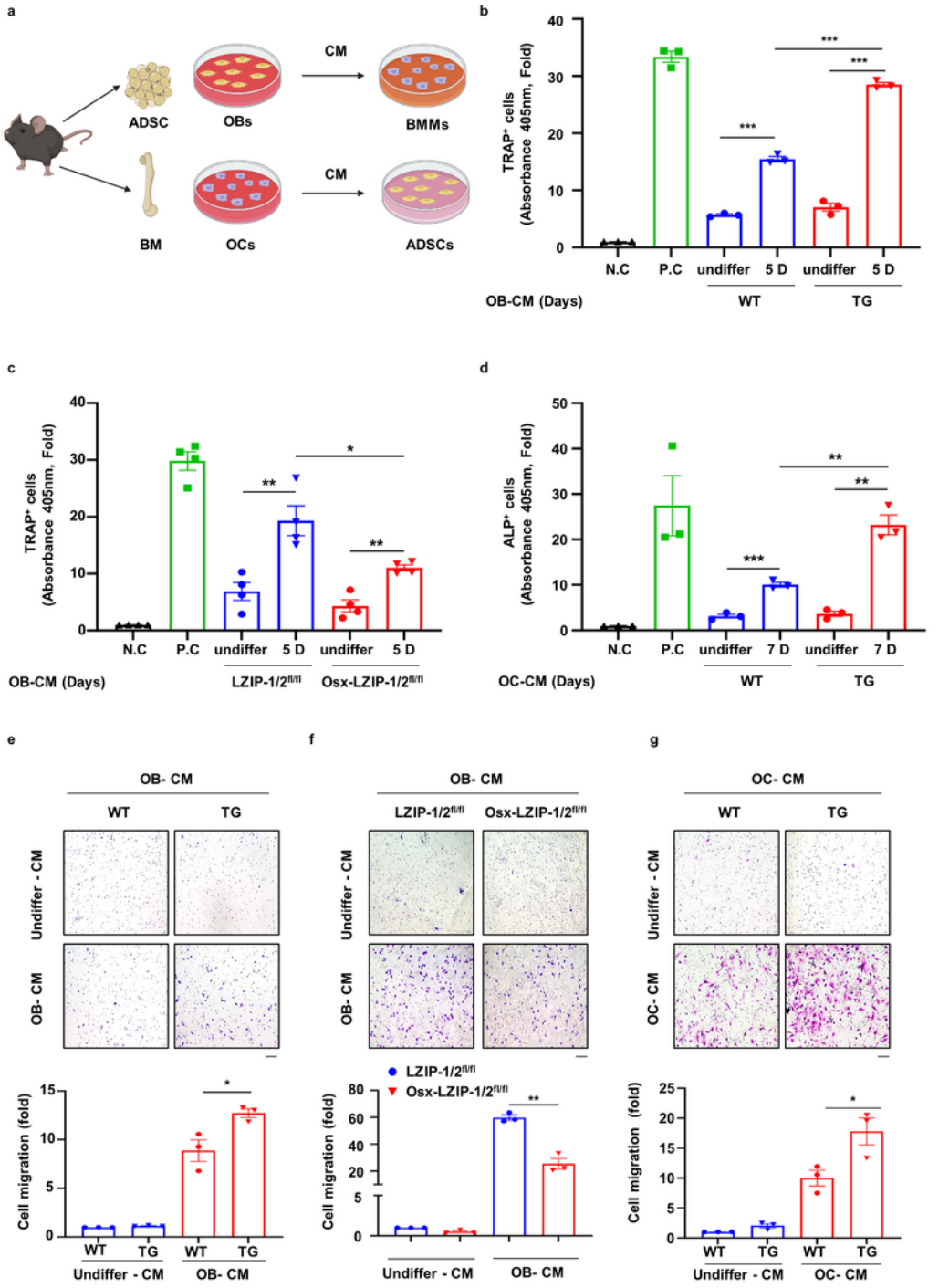

Figure 4

sLZIP functions as a modulator of the crosstalk between OBs and OCs. **a** ADSCs isolated from mice were seeded at a density of 8 × 10^4 cells/well in 12-well culture plates and differentiated into mature OBs for 5 and 7 days. CM was collected from mature OBs. BMMs isolated from mice were seeded at a density of 2 × 10^5 cells/well in 12-well culture plates and differentiated into mature OBs for 7 days. CM was collected from mature OCs. **b,c** BMMs isolated from WT mice were seeded at a density of 1 × 10^4 cells/well in 96-

well culture plates and cultured in α-MEM with OB-CM and 30 ng/mL M-CSF for 7 days. Cells were then subjected to TRAP staining. Negative control (N.C) cells were cultured in α-MEM with 30 ng/mL M-CSF for 7 days and positive control (P.C) cells were cultured in α-MEM with 30 ng/mL M-CSF and 50 ng/mL RANKL for 7 days. **d** ADSCs isolated from WT mice were seeded at a density of 1×10^4 cells/well in 96-well culture plates and exposed to OC-CM for 7 days. Cells were then subjected to ALP staining. **e,f** CM of mature OBs was collected from mice. BMMs (8×10^4 cells/well) derived from WT mice were plated on the insert of transwell plates. For migration assay, cells were stained with 0.05% crystal violet. Representative images were shown (Scale bar, 100 μm). Cells were counted from five randomly selected fields. **g** CM of mature OCs was collected from mice. ADSCs (2×10^4 cells/well) derived from WT mice were plated on the insert of transwell plates. For migration assay, cells were stained with 0.05% crystal violet. Representative images are shown (Scale bar, 100 μm). Cells were counted from five randomly selected fields. All experiments were repeated thrice independently. Error bars: mean ± SEM. *$p < 0.05$, **$p < 0.01$, ***$p < 0.001$ (unpaired, Two-tailed Student's *t*-test).

Figure 5.

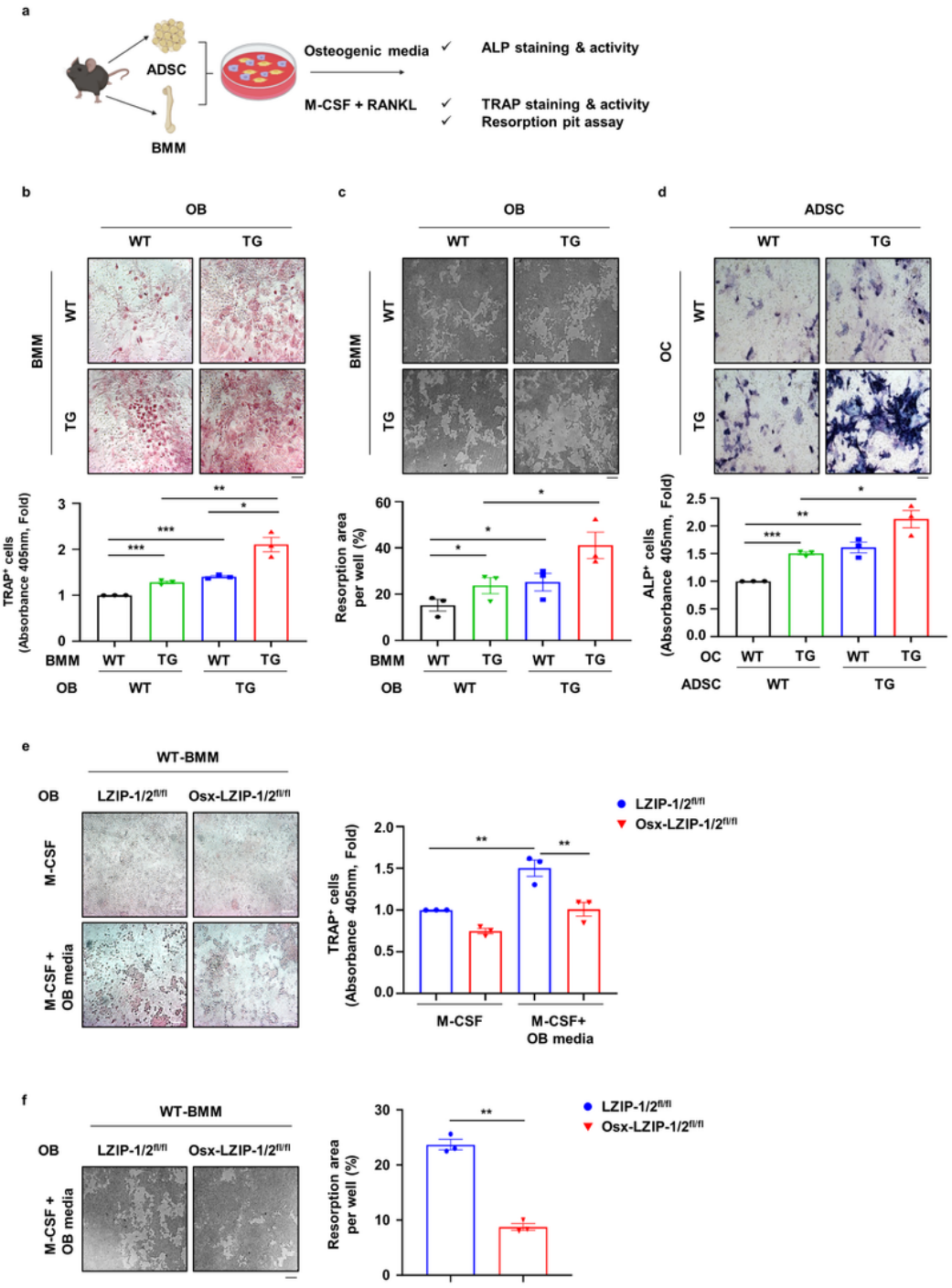

Figure 5

sLZIP modulates bone remodeling by regulating the crosstalk between OBs and OCs. **a** ADSCs and BMMs (1.5×10^4 cells/ well, ADSCs : BMMs = 1 : 1.5) were co-cultured in 96-well culture plates. One day after seeding, cells were cultured in osteogenic medium containing 30 ng/mL M-CSF or OC differentiation medium for 13 days. After differentiation, cells were subjected to TRAP and ALP staining using the TRACP/ALP double stain kit. **b** BMMs and ADSCs were isolated from WT and sLZIP TG mice. Cells were

subjected to TRAP staining using the TRACP stain kit. **c** Ten days after culture in osteogenic medium containing 30 ng/mL M-CSF, cells were detached using 5% bleach solution. Plates were washed with DDW and dried in a CO_2 incubator. Resorbed area was calculated using ImageJ. Five fields from each well were randomly selected for quantification. **d** BMMs and ADSCs were isolated from WT and sLZIP TG mice. The ALP stain kit was used for ALP staining. (E and F) BMMs and ADSCs were isolated from LZIP-$1/2^{fl/fl}$ and Osx-LZIP-$1/2^{fl/fl}$ mice. **e** The TRAP stain kit was used for TRAP staining of OCs in the co-culture system and the TRAP activity was measured at absorbance 405 nm. **f** Resorption area was calculated using ImageJ. All experiments were repeated thrice independently. Error bars: mean ± SEM. *$p < 0.05$, **$p < 0.01$, ***$p < 0.001$ (unpaired, Two-tailed Student's *t*-test).

Figure 6.

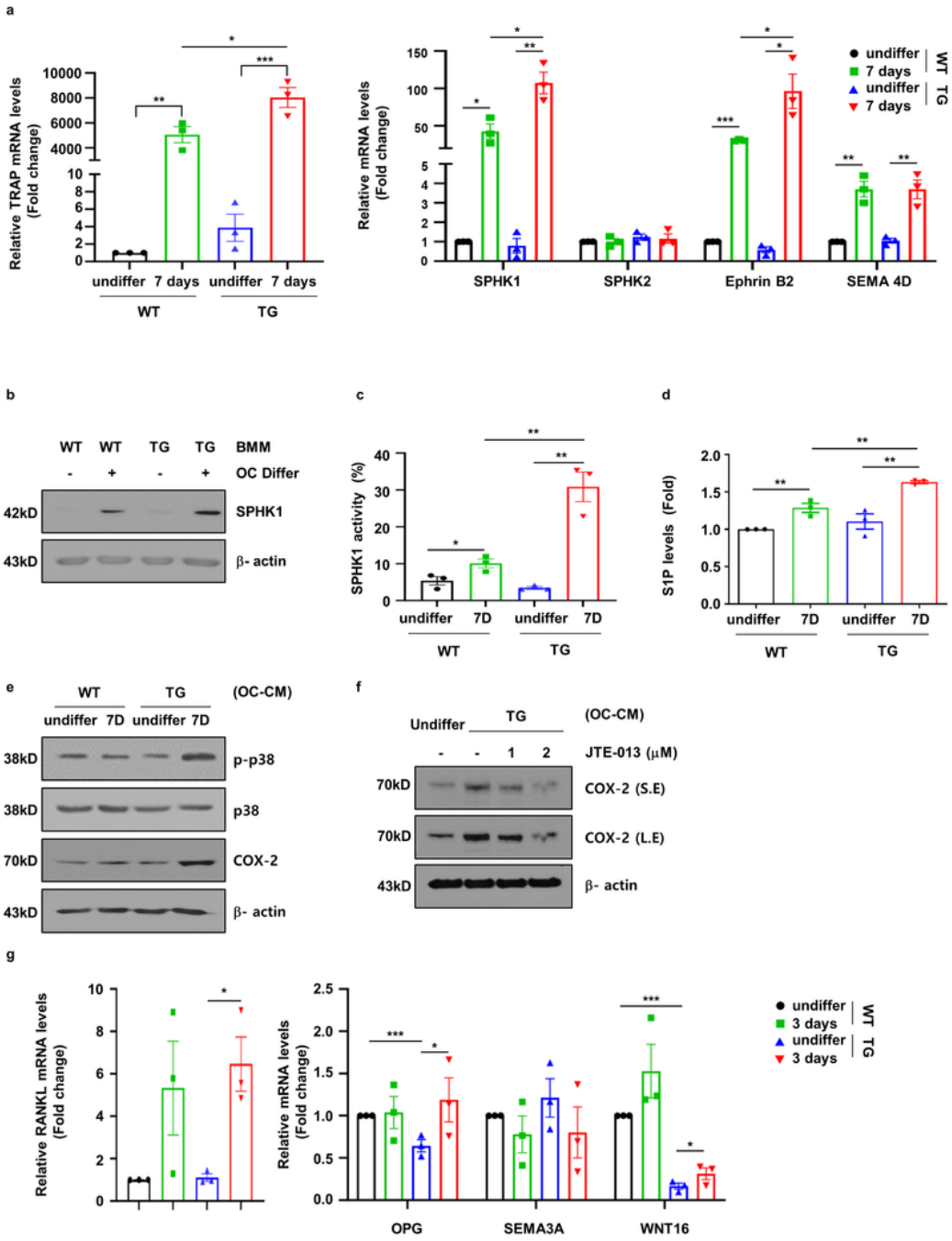

Figure 6

sLZIP regulates the crosstalk between OBs and OCs by inducing the coupling factors. **a-d** BMMs isolated from WT and sLZIP TG mice were mice were seeded at a density of 1.5×10^5 cells/well in 12-well culture plates and cultured for 7 days in α-MEM containing 50 ng/mL RANKL and 30 ng/mL M-CSF. **a** mRNA expression level was determined using qRT-PCR analysis. β-actin was used as an internal control. **b** Protein expression level was determined using western blotting. **c** SPHK1 activity was determined using

30 μg cell lysates. **d** S1P levels was analyzed using ELISA kit. **e,d** ADSCs derived from WT mice were exposed to differentiated OC-CMs from WT and sLZIP TG mice. Protein expression level was determined using western blotting. **f** ADSCs were cultured with OC-CM from TG and JTE-013 (0, 1, and 2 μM) for 24 h. Protein levels was detected using western blotting. β-actin was used as an internal control. **g** ADSCs derived from WT and sLZIP TG mice were seeded at a density of 8×10^4 cells/well in 12-well culture plates and differentiated into OBs for 3 days. mRNA expression level was determined by qRT-PCR analysis. All experiments were repeated thrice independently. Error bars: mean ± SEM. *$p < 0.05$, **$p < 0.01$, ***$p < 0.001$ (unpaired, Two-tailed Student's *t*-test).

Figure 7.

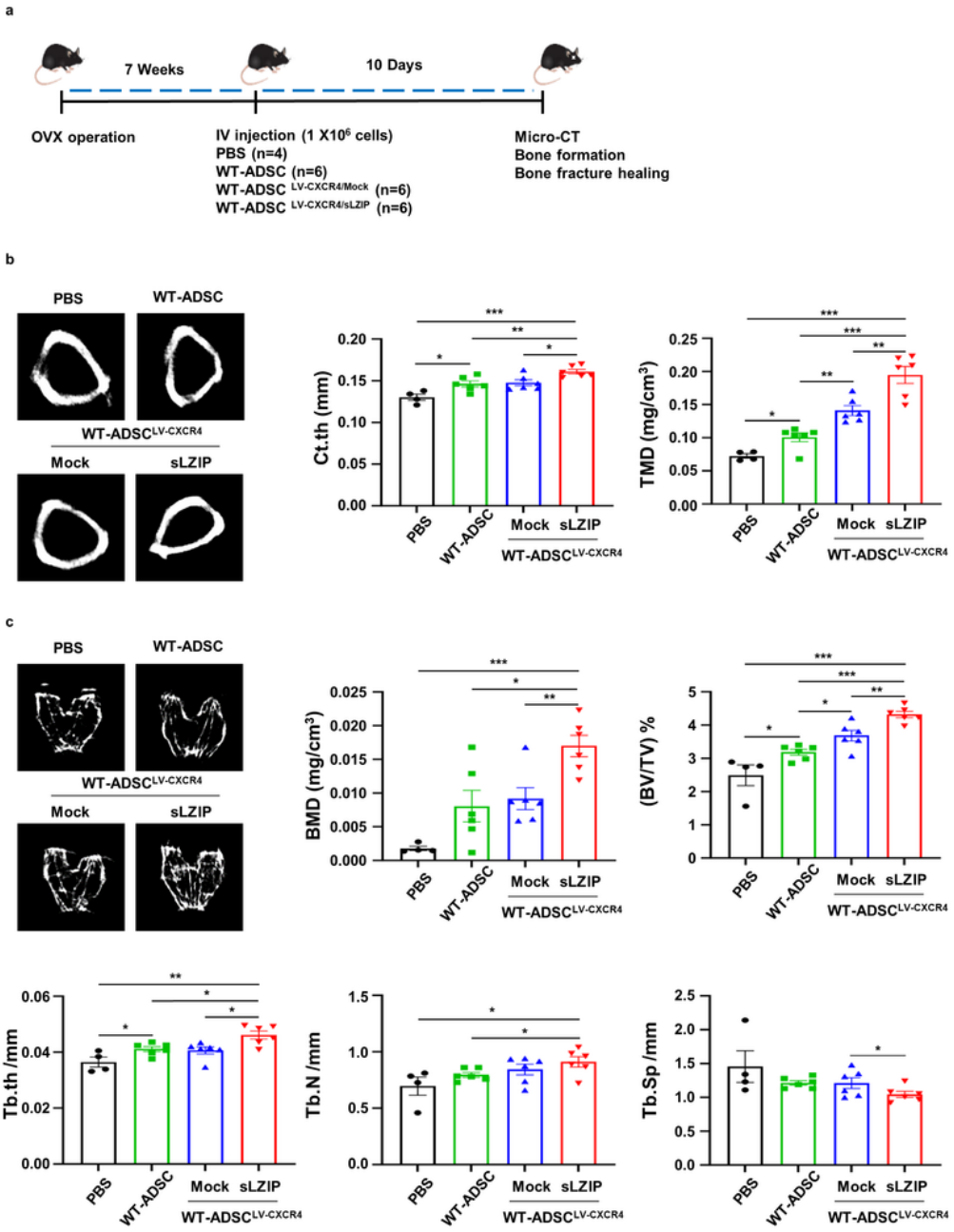

Figure 7

sLZIP overexpressing ADSCs promote bone formation in osteoporosis. **a** OVX surgery was performed using WT mice. After 7 weeks, each type of ADSC cells (1 ´ 10^6 cells/100 µL PBS) were intravenously injected into OVX mice. After 10 days, mice femur was analyzed using µCT. **b** Representative 2D images were obtained from µCT analysis. Quantification of Ct.Th and TMD were analyzed using the µCT program. **c** Representative two-dimensional images were generated from µCT analysis. BMD, BV/TV,

Tb.Th, Tb. N, and Tb.Sp were quantified using μCT. Error bars: mean ± SEM. *$p < 0.05$, **$p < 0.01$, ***$p < 0.001$ (unpaired, Two-tailed Student's *t*-test).

Figure 8.

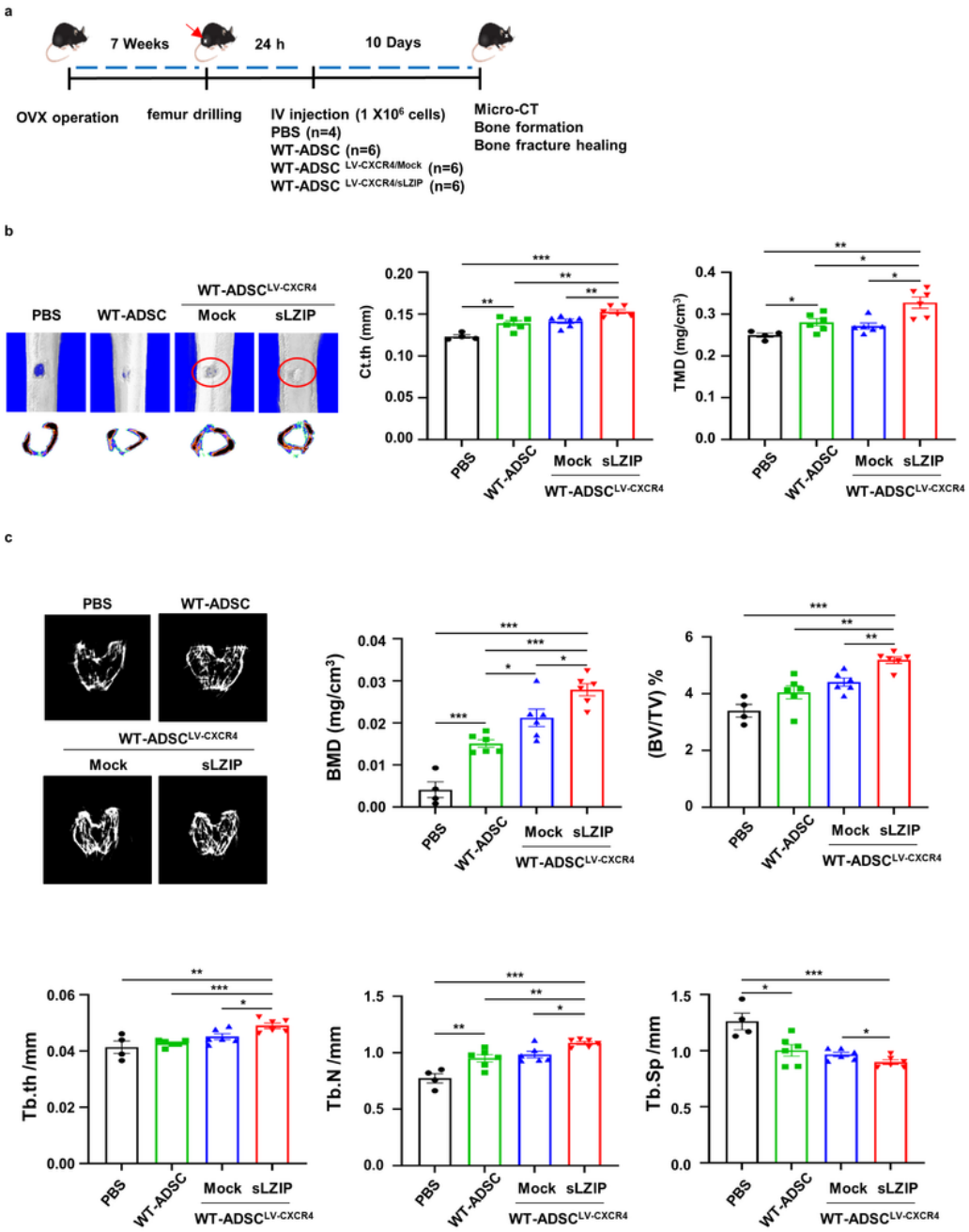

Figure 8

sLZIP overexpressing ADSCs promote bone repair in osteoporosis. **a** Eight-week-aged mice were used for OVX surgery. Seven weeks after surgery, mice were anesthetized and underwent surgery to drill holes in

the right femur. After 24 h, each type of ADSC cells (1 ´ 10^6 cells/100 µL PBS PBS) were intravenously injected into mice. After 10 days, mice femur was analyzed using µCT. **b** Representative two- and three-dimensional were generated from µCT analysis. Quantification of Ct.Th and TMD were analyzed using the µCT program. **c** Representative two-dimensional images were generated from µCT analysis. BMD, BV/TV, Tb.Th, Tb. N, and Tb.Sp were quantified using the µCT program. Error bars: mean ± SEM. *p < 0.05, **p < 0.01, ***p < 0.001 (unpaired, Two-tailed Student's t-test).

Figure 9.

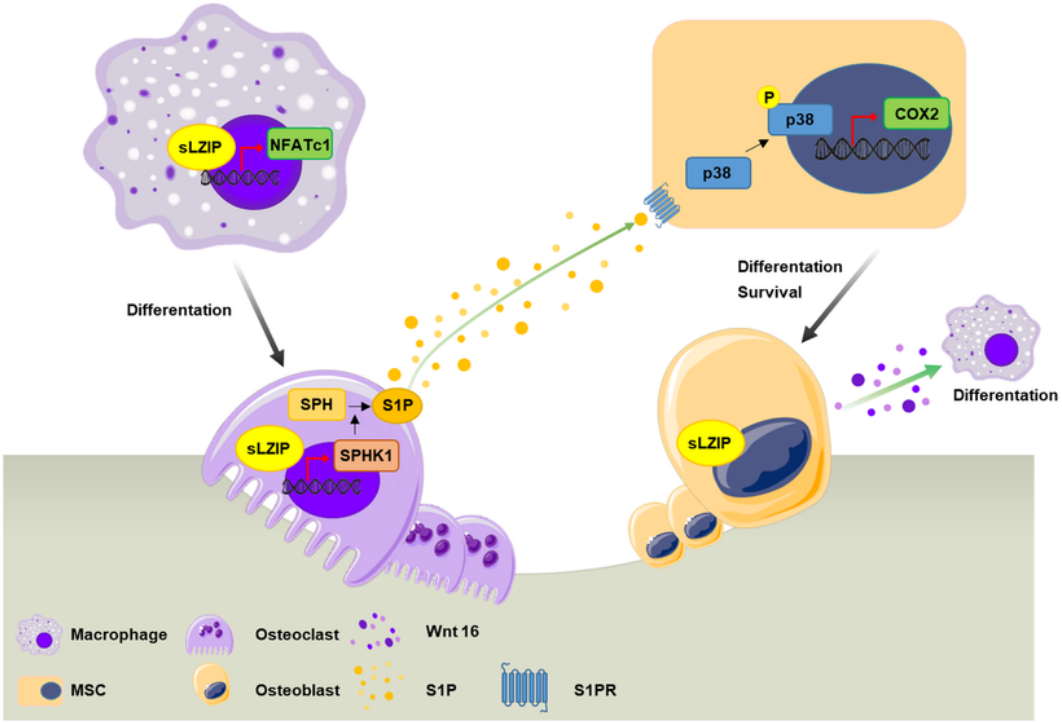

Figure 9

Legend not included with this version.

Supplementary Files

This is a list of supplementary files associated with this preprint. Click to download.

- BoneResSupplementaryinformation.docx